Tropical Cyclone Wind Retrievals from the Advanced Microwave Sounding Unit: Application to Surface Wind Analysis

KOTARO BESSHO

Japan Meteorological Agency/Meteorological Research Institute, Tsukuba City, Ibaraki, Japan

MARK DEMARIA

Office of Research and Applications, NOAA/NESDIS, Fort Collins, Colorado

JOHN A. KNAFF

Cooperative Institute for Research in the Atmosphere, Colorado State University, Fort Collins, Colorado

(Manuscript received 27 December 2004, in final form 4 August 2005)

ABSTRACT

Horizontal winds at 850 hPa from tropical cyclones retrieved using the nonlinear balance equation, where the mass field was determined from Advanced Microwave Sounding Unit (AMSU) temperature soundings, are compared with the surface wind fields derived from NASA's Quick Scatterometer (QuikSCAT) and Hurricane Research Division H*Wind analyses. It was found that the AMSU-derived wind speeds at 850 hPa have linear relations with the surface wind speeds from QuikSCAT or H*Wind. There are also characteristic biases of wind direction between AMSU and QuikSCAT or H*Wind. Using this information to adjust the speed and correct for the directional bias, a new algorithm was developed for estimation of the tropical cyclone surface wind field from the AMSU-derived 850-hPa winds. The algorithm was evaluated in two independent cases from Hurricanes Floyd (1999) and Michelle (2001), which were observed simultaneously by AMSU, QuikSCAT, and H*Wind. In this evaluation the AMSU adjustment algorithm for wind speed worked well. Results also showed that the bias correction algorithm for wind direction has room for improvement.

1. Introduction

Tropical cyclone (TC) wind observations are obtained in a variety of ways. In situ surface observations include those from surface stations, buoys, and ships, and upper-air observations include those from radiosondes, aircraft reconnaissance, and global positioning system (GPS) dropsondes. Winds can also be measured using remote sensing such as Doppler radar, microwave scatterometers, and microwave radiometers. Microwave scatterometers provide the well-known sea surface wind observations from the SeaWinds scatterometer on the National Aeronautics and Space Administration (NASA) Quick Scatterometer (QuikSCAT) satellite. Microwave radiometers on satellites, such as the Special Sensor Microwave Imager (SSM/I) on Defense Meteorological Satellite Program (DMSP), the Tropical Rainfall Measuring Mission (TRMM) Microwave Imager (TMI), and the Advanced Microwave Scanning Radiometer Earth Observing System (EOS) (AMSR-E) on *Aqua*, can only observe wind speed over the ocean. Wind speed and direction above the surface can be retrieved from sequential images from geostationary satellites using feature-tracking methods. The traditional method for estimating the TC maximum wind is the Dvorak technique (Dvorak 1975, 1984).

Satellite microwave soundings are also used for estimation of TC winds. The first studies of TC surface wind speed estimation using microwave soundings are by Kidder et al. (1978, 1980). They describe a statistical method to estimate surface wind speed from the 55.45-GHz channel of the Scanning Microwave Spectrometer on *Nimbus-6*. In these papers, outer surface wind

Corresponding author address: Kotaro Bessho, Japan Meteorological Agency/Meteorological Research Institute, Tsukuba City, Ibaraki 305-0052, Japan.
E-mail: kbessho@mri-jma.go.jp

speeds were calculated by assuming gradient balance and using a regression between central pressure and the 55.45-GHz temperature anomaly, from which the temperature and size of the hurricane warm core can be estimated. Their works were followed by articles from Velden and Smith (1983), Velden (1989), and Velden et al. (1991) who expanded the use of high-resolution data from the Microwave Sounding Unit (MSU) on National Oceanic and Atmospheric Administration (NOAA) polar-orbiting satellites. Merrill (1995) provided a new algorithm to more accurately estimate the TC upper-tropospheric warm anomaly from 55-GHz microwave observations.

Recently, new microwave sounding systems were included on *NOAA-15*, *-16*, and *-17*. The Advanced Microwave Sounding Unit (AMSU) is a successor of the MSU, and its applicability to TC analysis was shown by Kidder et al. (2000) and Knaff et al. (2000). The best horizontal resolution of AMSU is 48 km, which is 2 times that of MSU. AMSU has also a finer vertical resolution with 15 channels for atmospheric temperature sounding. Using this new instrument, there are several techniques to estimate wind speed in TCs. A recent extended version of the work of Kidder et al. (1978) is described by Brueske and Velden (2003). They calculated minimum sea level pressure from the brightness temperature of the AMSU 54.96-GHz channel with the maximum likelihood regression algorithm developed by Merrill (1995).

Demuth et al. (2004, hereinafter D04) chose an alternate approach to the problem of TC intensity estimation from AMSU. They calculated 15 physical estimators from atmospheric temperature, geopotential height, surface pressure, and the gradient wind around TCs retrieved from AMSU brightness temperatures. These estimators are the input to a multiple regression analysis for TC intensity and wind structure. The National Hurricane Center (NHC) best track was used for the ground truth values of intensity (maximum 1-min-sustained surface winds and minimum sea level pressure), and the wind structure was measured by the radii of 34-, 50-, and 64-kt winds in four quadrants relative to the TC center (1 kt $\approx$ 0.5144 m s^{-1}). Spencer and Braswell (2001) used a somewhat similar statistical approach to estimate the TC maximum wind from several AMSU channels.

In the studies described above, single TC parameters, such as maximum surface wind speed, central pressure, or wind radii, were estimated. In some cases, subsets of the wind field are estimated such as the gradient wind as a function of radius in D04, but none of the AMSU TC retrieval methods described above recovers the entire wind field. In this paper a new method to estimate the two-dimensional TC surface wind field is described. The method uses the nonlinear balance equation (Charney 1955) to estimate the three-dimensional wind fields from the AMSU-retrieved mass field. The nonlinear balance winds at the lowest reliable level (850 hPa) are then used to estimate the surface wind. In section 2 the three-dimensional wind retrieval is briefly described. The datasets used in this study are described in section 3. In section 4 the wind fields at 850 hPa are compared with surface wind fields from QuikSCAT and H*Wind analyses from the NOAA Hurricane Research Division (HRD) of the Atlantic Oceanography and Meteorology Laboratory (AOML) (Powell et al. 1998). Based upon this comparison, an algorithm to convert the 850-hPa AMSU winds to surface winds is developed. In section 5 this simple algorithm is validated in two cases that were simultaneously observed by AMSU, QuikSCAT, and H*Wind. The results are discussed and summarized in sections 6 and 7.

The algorithm described in this paper can be used to estimate the horizontal distribution of sea surface wind in and around TCs from AMSU brightness temperature data. The estimated wind fields have potential application to the improvement of TC warnings and the initialization of numerical TC prediction models.

2. Three-dimensional AMSU wind retrieval

The AMSU wind retrieval is a generalization of the gradient wind retrieval described by D04. The temperature on an evenly spaced latitude–longitude grid from 50 to 920 hPa is determined in the same way as in D04. A statistical retrieval is applied to the AMSU-A radiances to determine the temperature profile and the vertically integrated cloud liquid water (CLW), which are then interpolated from the instrument "footprint" locations to a 0.2° latitude $\times$ 0.2° longitude grid centered on the storm. Empirical corrections are applied to the temperature retrievals to help to account for artificial cooling resulting from attenuation by liquid water and scattering by ice (D04; Linstid 2000). Cases are restricted to those in which the storm center was within 700 km of the center of the AMSU swath, ensuring that there is adequate data coverage over the 12° $\times$ 12° analysis domain. Using a National Centers for Environmental Prediction (NCEP) global analysis as a lower boundary condition for surface pressure at the domain boundaries, the hydrostatic equation is integrated upward to 50 hPa using the AMSU temperatures to give the geopotential height as a function of pressure at the lateral boundaries. Virtual temperature effects are neglected in all of the hydrostatic integrations. Under the assumption that 50 hPa is above the storm circulation,

a smoothness condition is applied to give the geopotential height over the entire domain at 50 hPa. The hydrostatic equation is then integrated downward to give the three-dimensional height field. In D04 this height field is azimuthally averaged relative to the storm center and the gradient wind equation is used to determine the wind at each pressure level as a function of radius.

For the three-dimensional winds the gradient wind equation is replaced by the nonlinear balance equation (Charney 1955). On a midlatitude beta plane this equation can be written as

$$u_x u_x + 2v_x u_y + v_y v_y - \zeta(f + \beta y) + \beta u + \nabla^2 \phi = 0, \tag{1}$$

where u and v are the nondivergent horizontal wind components, f and β are the Coriolis parameter and its northward gradient, respectively, evaluated at the domain center, ϕ is the geopotential, ∇^2 is the horizontal Laplacian operator, and subscripts x and y represent eastward and northward derivatives. The properties of the nonlinear balance equation are discussed in detail by Paegle and Paegle (1976) and Kasahara (1982). An important property of (1) is that it is an elliptic equation provided that

$$f^2 + 2\nabla^2 \phi + 2\beta u < 0. \tag{2}$$

A number of iterative methods have been developed to solve (1) for the nondivergent wind field given the geopotential field (e.g., Kasahara 1982; Iversen and Nordeng 1982). However, it was found that these conventional solution methods did not converge for some of the stronger TC cases, primarily because of violations of (2) over small regions near the storm center. For this reason, a least squares method was used to solve (1).

For the least squares solution, (1) is first written in finite-difference form. Then, the residual of the finite-difference form of (1) at each grid point is defined as R_{ij}. The mean square residual is defined as

$$L = \sum_{i=2}^{I-1} \sum_{j=2}^{J-1} R_{ij}^2. \tag{3}$$

The summation is over all of the points in the analysis domain except the lateral boundaries. At the boundaries, u and v are determined from the NCEP analyses. At all interior points, u and v are determined by minimizing (3). The minimization is performed using a gradient-descent method, where the gradient of L with respect to u and v at each analysis point is calculated by taking the derivative of (3) after substitution of the finite-difference form of (1). The gradient-descent algorithm converges much more slowly than the more standard iterative solutions but is much more robust, especially for the stronger TCs. The method provides u and v at each pressure level from 50 hPa to the surface.

Because the AMSU radiances are attenuated in areas with large amounts of liquid water, the temperature retrievals are less reliable in the low levels near the storm center. A method to partially correct for this problem is included in the temperature retrieval algorithm as described by D04. However, the wind retrievals are still considered less reliable below 850 hPa, so the AMSU winds at 850 hPa will be used in the remainder of the paper.

3. Data

a. AMSU

This study utilizes the AMSU brightness temperature data from *NOAA-15* and *-16*, which are archived in a Cooperative Institute for Research in the Atmosphere (CIRA) database for TCs from 1999 to 2002. The cases were restricted to those of hurricane strength (maximum surface winds of at least 33 m s^{-1}). The data collection process is the same as that described in D04, in which the AMSU observations around all TCs being forecast by NHC were saved at 6-h intervals. If new data were available at a 6-h period and the storm center was within 700 km of center of the AMSU swath, the case was saved in the archive. This procedure resulted in about one case per storm per satellite per day.

b. QuikSCAT

QuikSCAT sea surface wind data archived on a file transfer protocol (FTP) site of Remote Sensing Systems (RSS) were collected for comparison with the AMSU wind data. The SeaWinds instrument on QuikSCAT launched in June 1999 is a Ku-band (i.e., a frequency near 14 GHz) radar. It works as a scatterometer to transmit a radar pulse down to the sea surface and measures the power that is scattered back. The power of the backscattered radiation is proportional to the ocean surface roughness, which is correlated with the near-surface wind speed and direction. QuikSCAT can easily detect a TC as a closed circulation in the surface winds on the ocean (Katsaros et al. 2001).

In the RSS database, sea surface wind was retrieved from QuikSCAT with a geophysical model function called Ku-2001 (Wentz et al. 2001). The wind speed and direction at a height of 10 m are retrieved from measurements of the power of the backscattered radiation. The wind QuikSCAT data correspond to surface winds with a time averaging period of 8–10 min.

c. H*Wind

As will be shown in detail later, both the AMSU and QuikSCAT winds have limitations. To provide "ground truth," H*Wind surface wind field analyses were obtained from the HRD ftp site. H*Wind was developed to integrate many kinds of wind data such as in situ surface observations, aircraft reconnaissance, GPS dropsonde, and remote sensing observations, into a consistent surface wind field (Powell et al. 1998). All data are quality controlled and processed to conform to a common framework for height (10 m), exposure (marine or open terrain over land), and averaging period (maximum 1-min-sustained wind speed) using results from micrometeorology and wind engineering (Powell et al. 1996; Powell and Houston 1996). H*Wind analyses are provided on an FTP server for research purposes, and to NHC hurricane specialists for forecast applications on a regular 3- or 6-h schedule consistent with NHC's warning and forecast cycle. The spatial resolution of H*Wind analyses used in this study vary between 2.8 and 8.4 km.

The surface wind data synthesized into H*Wind include data from ships, buoys, coastal platforms, and surface aviation reports. Aircraft reconnaissance data are adjusted to the surface with a planetary boundary layer model (Powell 1980). Remote sensing observations in H*Wind can include surface wind speed estimates from microwave imagers such as SSM/I and TMI on polar-orbiting satellites, surface wind estimates from scatterometers on European Remote Sensing Satellite (ERS) and QuikSCAT, low-level cloud drift winds from Geostationary Operational Environmental Satellites (GOES), and, if available, step-frequency microwave radiometer measurements of surface winds from NOAA WP-3D aircraft. In this paper the H*Wind analyses are used for a comparison with AMSU and QuikSCAT wind estimates. To maintain independence among the three types of wind estimates, the H*Wind analyses that did not include QuikSCAT observations were used in this study.

d. AMSU–QuikSCAT comparison cases

Fifty-seven cases were chosen for comparison of the AMSU and QuikSCAT wind fields. The time differences for the matching cases were less than 1.5 h. The cases in which there were landmasses such as continents or large islands in the analysis region were excluded. Footprints in which the QuikSCAT rain flags were marked for strong rain attenuation were also excluded from comparison. Using a Barnes analysis (Barnes 1964), the QuikSCAT winds were interpolated to the 12° latitude × 12° longitude AMSU analysis grid. The comparison was then restricted to only those grid points within 500 km of the TC center.

e. AMSU–H*Wind comparison cases

For comparison of the AMSU 850-hPa wind field with the H*Wind surface wind field, 16 cases were found in which the time difference was less than 3 h. Similar to the comparisons between AMSU and QuikSCAT, cases in which continents or large islands were located in analysis region were excluded. H*Wind has large (8° latitude × 8° longitude) or small (4° latitude × 4° longitude) analysis domains. In this study the H*Wind data in the larger analysis domain were used. Similar to the QuikSCAT data, the H*Wind analyses were interpolated to the AMSU retrieval grid points using a Barnes analysis, and the comparisons were restricted to grid points within 500 km of the storm center. H*Wind speeds were converted from 1- to 10-min averages by dividing by 1.1 (Powell et al. 1996).

f. AMSU–QuikSCAT–H*Wind comparison cases

Out of the 57 AMSU cases with matching QuikSCAT data and the 16 cases with matching H*Wind data, there are two cases for which all three wind fields are available. These cases were set aside for independent validation of the algorithm to convert the AMSU 850-hPa winds to surface values. Thus, all of the analysis described in the next section includes 55 QuikSCAT cases and 14 H*Wind cases.

Table 1 shows statistics of wind parameters and central pressure in the comparison cases. Statistics of maximum wind and central pressure can be calculated from all comparison cases, but wind radii of 34, 50, and 64 kt for four directions (northeast, southeast, southwest, northwest) can be averaged only from the cases in which those wind speed thresholds are archived. From the upper table, the maximum wind speeds in each set of comparison cases have about the same average value ($\sim$30 m s^{-1}). However, from the lower table, the AMSU–H*Wind comparison cases have 1.5–2 times the wind radii of AMSU–QuikSCAT comparison cases.

Figure 1 shows the locations of TCs in the comparison cases. This figure shows that TCs in AMSU–QuikSCAT comparison cases were distributed over all western Atlantic Ocean and eastern Pacific Ocean basins except for the Caribbean Sea and Gulf of Mexico. On the other hand, TCs in the AMSU–H*Wind comparison cases are restricted to the far western side of the Atlantic basin because they all include aircraft reconnaissance data. According to Table 1, the average central pressure for the AMSU–H*Wind cases is 983 hPa as compared with 992 hPa for the AMSU–QuikSCAT

TABLE 1. Statistics of the TC wind parameters and central pressures in the comparison cases. The upper table shows the maximum wind speed and central pressure statistics, and the lower table shows the average radii of 34-, 50-, and 64-kt winds for the four quadrants (northeast, southeast, southwest, northwest) relative to the storm center.

	Avg	Max	Min	Std dev
AMSU–QuikSCAT (55 cases)				
Max wind speed ($m\ s^{-1}$)	28	72	13	14
Central pressure (hPa)	992	1010	921	19
AMSU–H*Wind (14 cases)				
Max wind speed ($m\ s^{-1}$)	35	59	10	15
Central pressure (hPa)	983	1013	924	25
	Northeast	Southeast	Southwest	Northwest
AMSU–QuikSCAT (45 cases)				
34-kt wind radii (km)	173	151	125	146
50-kt wind radii (km)	75	56	51	63
64-kt wind radii (km)	24	22	17	22
AMSU–H*Wind (13 cases)				
34-kt wind radii (km)	269	221	177	209
50-kt wind radii (km)	158	100	89	108
64-kt wind radii (km)	63	37	33	50

cases. The storms in H*Wind cases tend to be more mature than in QuikSCAT cases. The uneven spatial distribution of the TCs in H*Wind cases probably explains the wind radii difference between the AMSU–H*Wind and AMSU–QuikSCAT comparison cases mentioned above.

4. Comparison of AMSU 850-hPa winds with QuikSCAT and H*Wind

Figure 2 shows scatterplots of wind speed and direction from the 850-hPa AMSU winds and the QuikSCAT surface wind field (Fig. 2a) and the H*Wind surface wind field (Fig. 2b) for the matching cases. The QuikSCAT comparison includes 84 576 grid points from the 55 cases, and the H*Wind comparison includes 22 217 grid points from the 14 matching cases. Statistics of the comparisons are summarized in Table 2.

Figure 2a shows that the QuikSCAT surface wind speed reached almost 60 $m\ s^{-1}$ but the AMSU wind speed only reaches about 40 $m\ s^{-1}$. The new RSS QuikSCAT retrieval is supposed to measure surface winds above 30 $m\ s^{-1}$ (Wentz et al. 2001). Figure 2a shows that some estimates are considerably higher than 30 $m\ s^{-1}$. The maximum wind speed differences are because of many factors, such as the very different way in which the winds are estimated, geophysical noise resulting from rain attenuation and ice scattering, and the temporal variability of wind speed. However, the biggest reason for the difference is considered to be the horizontal resolution difference between AMSU and QuikSCAT. According to Quilfen et al. (1998), the

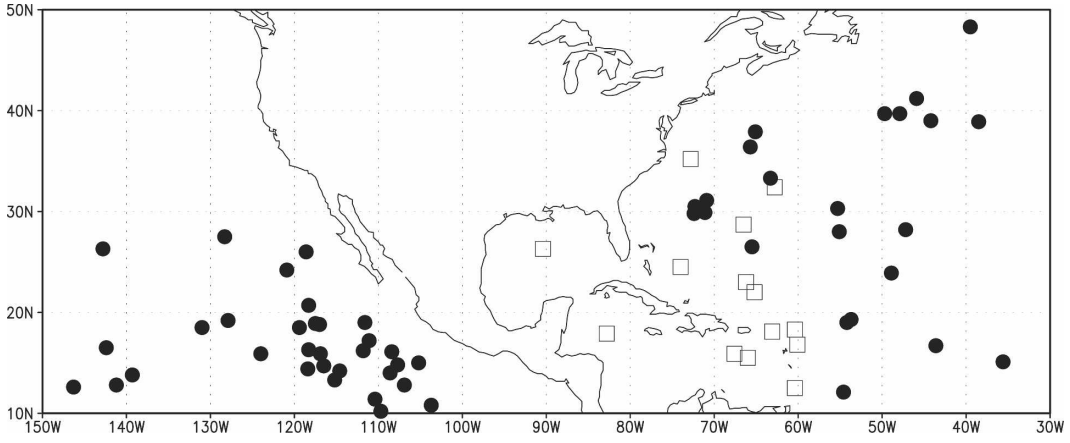

FIG. 1. Locations of TCs in the comparison cases. Filled circles are locations in the comparison cases for AMSU and QuikSCAT and open squares are those for AMSU and H*Wind.

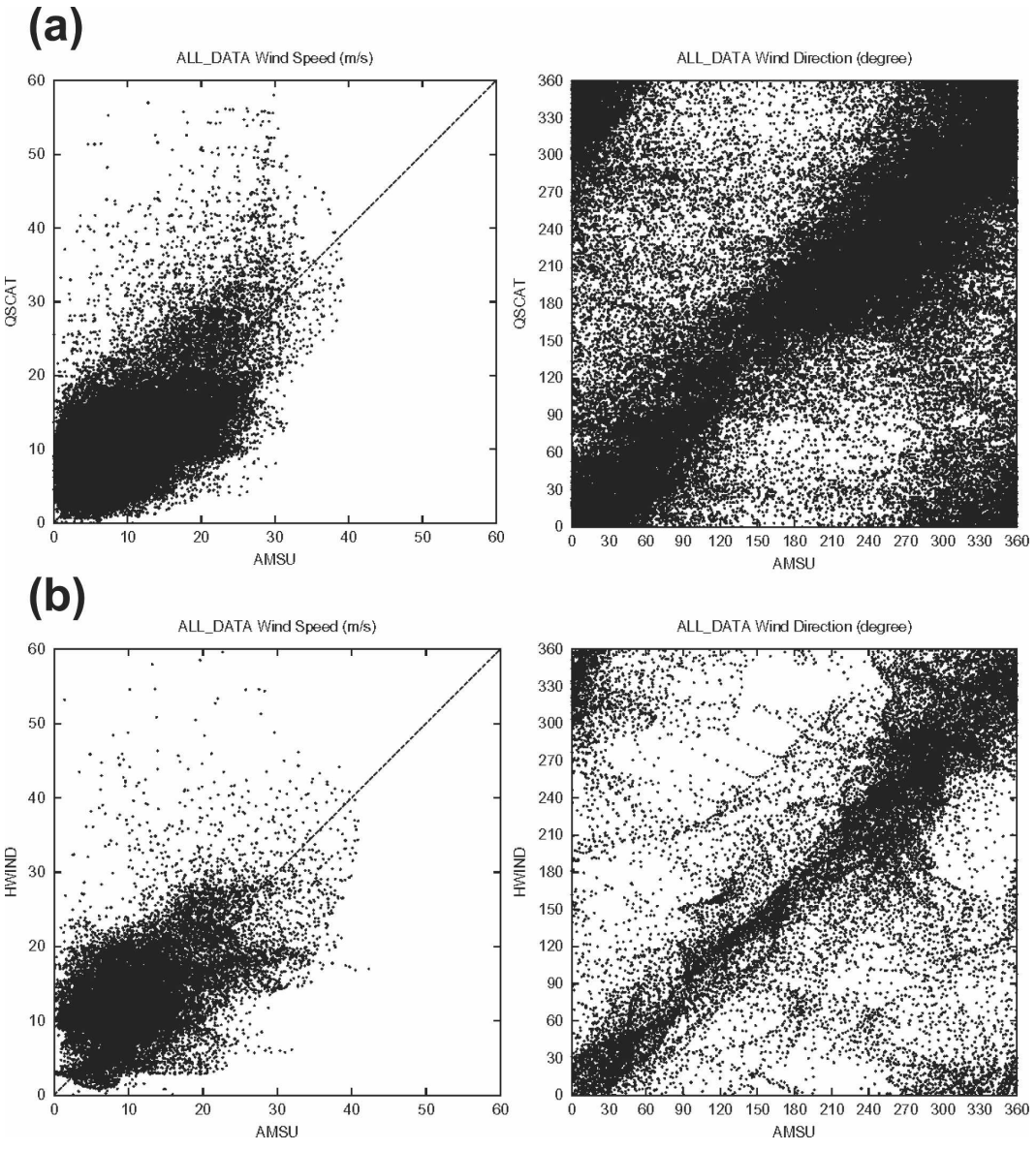

FIG. 2. Scatter diagrams of (a) AMSU wind at 850 hPa vs QuikSCAT surface wind, and (b) AMSU wind at 850 hPa vs H*Wind surface wind. The diagrams on the left side are for wind speed, and the diagrams on the right side are for wind direction.

fine-horizontal-resolution data of the scatterometer data (ERS in their case) enable the detection of fairly higher wind speeds in TCs. The finest AMSU horizontal resolution is 48 km, while QuikSCAT has a resolution of 25 km. Thus, QuikSCAT can better resolve the inner-core region of TCs, which is consistent with Fig. 2a in the high-wind regime. Except for the grid points in which the QuikSCAT wind speed is much higher than AMSU, most of the points are spread evenly around the dotted line in Fig. 2a where the AMSU wind speed is equal to the QuikSCAT wind speed. As shown in

TABLE 2. Statistics of the comparisons of AMSU wind speed and direction at 850 hPa with QuikSCAT or H*Wind; MAD: mean absolute difference; COR: correlation coefficient between AMSU and QuikSCAT, or H*Wind.

	Bias	MAD	COR
QuikSCAT			
Wind speed (m s^{-1})	−1.49	4.10	0.609
Wind direction (°)	14.8	42.7	0.519
H*Wind			
Wind speed (m s^{-1})	−0.59	4.91	0.533
Wind direction (°)	13.4	38.1	0.621

Table 2, the AMSU wind speed bias relative to QuikSCAT is -1.5 m s^{-1}, and the mean absolute difference (MAD) is almost 4 m s^{-1}. The correlation coefficient between the AMSU and QuikSCAT wind speeds is 0.609.

Similar results are found in the comparison of AMSU winds with H*Wind surface winds as shown in Fig. 2b. The maximum wind speed of H*Wind is almost 60 m s^{-1}, but the maximum AMSU wind speed is only about 40 m s^{-1}. This speed difference is also related to differing horizontal resolution. As mentioned previously, the resolution of the H*Wind analyses ranged from 2.8 to 8.3 km in the 14 comparison cases, which was necessary to resolve the aircraft data. The bias of the AMSU wind speed relative to H*Wind is -0.6 m s^{-1} in Table 2. The MAD of the wind speed is about 5 m s^{-1}, which is larger than the MAD between AMSU and QuikSCAT, and the correlation coefficient of AMSU and H*Wind wind speed is 0.533, which is smaller than that of AMSU versus QuikSCAT.

The statistics of wind direction differences are complicated by the fact that 0° and 360° have the same meaning. Recently, "circular statistics" were developed (Fisher 1993; Jammalamadaka and SenGupta 2001) to handle this problem. Statistical parameters such as the mean absolute difference, standard deviation, bias, and correlation coefficient for wind direction in this paper were calculated by circular statistics.

As shown in Fig. 2a and Table 2, the MAD of wind direction between AMSU and QuikSCAT is about 40° and the bias is 14.8°. The directional bias was defined as AMSU minus QuikSCAT, which indicates that the AMSU wind direction is larger than the mean QuikSCAT wind direction. Assuming cyclonic flow, the QuikSCAT surface wind direction turns inward toward the hurricane center by about 15° from the direction of the AMSU wind at 850 hPa. This result is consistent with previous studies of TC wind structure. For example, Frank (1977) found mean inflow angles within 200–700 km of northwest Pacific TCs to be 23°–25° at the surface and 3°–8° at 850 hPa. Thus, the surface winds turned inward about 19° relative to the 850-hPa winds, which is similar to the bias of AMSU wind direction relative to the QuikSCAT wind direction.

Similar results are found in the comparison of AMSU and H*Wind wind directions, as shown in Table 2. The MAD is about 40° and the bias is consistent with the expected inflow angles at 850 hPa and the surface. The large mean absolute differences and biases can be seen in the scatterplots of wind directions in Fig. 2b. The correlation coefficient between AMSU and H*Wind wind directions is better than that for the comparison of AMSU with QuikSCAT. This improved correlation is probably because of the fact that the QuikSCAT wind directions also sometimes have substantial errors.

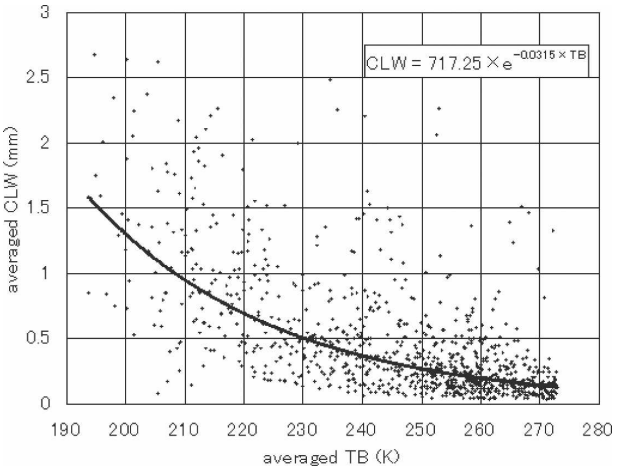

FIG. 3. Scatter diagram of tangentially averaged T_B vs azimuthally averaged CLW. The solid line shows exponential regression curve and the formula in the diagram shows its equation.

As briefly described in section 2, empirical adjustments are applied to help to correct the AMSU temperature soundings for attenuation by liquid water and scattering by ice. Although these corrections improve the retrievals as described by D04, there are still errors resulting from these effects, especially in regions of deep convection near the storm centers. To further investigate this issue, the AMSU wind retrievals will be stratified as a function of convective activity. For this purpose, the AMSU-retrieved CLW will be used as a proxy for convection.

Before stratifying the AMSU wind comparisons, the AMSU-retrieved CLW is compared with GOES infrared brightness temperatures (T_B) to provide some physical insight into the accuracy of the CLW values. For this purpose the GOES channel-4 (10.7 μm) T_B for the 55 AMSU–QuikSCAT comparison cases were obtained from an archive at CIRA. Because the GOES data are available at time intervals that are usually no longer than 0.5 h, the GOES data are very close in time to the AMSU data. The AMSU CLW values and GOES T_B were azimuthally averaged at 20-km radial intervals from the TC centers. This procedure resulted in 984 points with T_B colder than 273 K. If T_B were warmer than 273 K, the point was regarded as a near-surface sea or land temperature and was not included in the comparison.

Figure 3 shows a scatterplot of the azimuthally averaged T_B versus CLW, where an exponential regression curve is shown by a solid line. The determination coefficient of this curve is 0.426. As shown by Negri and Adler (1993), a T_B value of 235 K is often used as a

threshold for the identification of convective areas. From the regression curve in Fig. 3, a CLW value of 0.44 mm corresponds to a T_B value of 235 K. Thus, CLW = 0.44 mm will be used as a threshold for separating convective and nonconvective points in the AMSU analysis domain. Generally, CLW in convective clouds is larger than that in stratiform clouds and CLW has larger values in more developed convective clouds. If CLW $\geq$ 1.32 mm, the region is regarded as being "highly" convective. From the regression curve in Fig. 3, a CLW value of 1.32 mm corresponds to a T_B value of 200 K.

Figure 4 (left column) shows scatter diagrams of the AMSU–QuikSCAT wind differences versus AMSU wind speeds, stratified into nonconvective, convective, and highly convective regions. In each scatterplot least squares linear regressions are shown by dotted lines. Rain-flagged QuikSCAT data were detected by microwave brightness temperature observations from SSM/I and TMI (Wentz et al. 2001). On the other hand, convective and highly convective region were estimated from the value of AMSU CLW. As already mentioned above, QuikSCAT data with strong rain flags were excluded in this analysis, but there are still convective and highly convective regions because of the difference of these two estimation methods. The correlation coefficients, the slopes, and intercepts of the regression lines for each scatterplot in Fig. 4 are shown in Table 3. For all three stratifications on the left side of Fig. 4 there is a positive correlation between the AMSU winds and the AMSU–QuikSCAT difference. The *y* intercept for the highly convective region is the largest (-18 m s^{-1}), which indicates the largest bias of the AMSU wind speeds relative to the QuikSCAT speeds for the low AMSU wind speed cases. The *y* intercepts for the nonconvective and convective regions are also negative but are considerably smaller in magnitude than for the highly convective cases. The threshold values of AMSU wind speed between negative and positive AMSU–QuikSCAT differences also increases with each CLW stratification. For high values of AMSU wind speed in Fig. 4 the AMSU values are on average higher than the QuikSCAT winds, which is expected because QuikSCAT measures at the surface but AMSU is at 850 hPa.

Results similar to those described above are found in comparisons between AMSU wind speed at 850 hPa and the AMSU–H*Wind differences as shown in the Fig. 4 (right column) and Table 3. In the comparisons with H*Wind the correlation coefficients in all CLW categories are above 0.60. The linear regressions have almost the same slopes ($\sim$0.60), and intercepts range from -7.6 to -12.2 m s^{-1}. In the highly convective areas, the intercept in the AMSU–H*Wind difference is less than that for the AMSU–QuikSCAT difference.

Figure 5 shows the dependency of the wind direction difference between AMSU wind and QuikSCAT on AMSU wind speed. The mean and standard deviation of the wind direction differences in 5 m s^{-1} AMSU wind speed intervals are also shown in Fig. 5. For low AMSU wind speeds ($<$10 m s^{-1}), the wind direction differences vary widely from $-180°$ to $+180°$. For AMSU wind speeds greater than 10 m s^{-1}, the standard deviations of wind directional differences decrease and converge to near zero. The averaged differences of wind direction range from 12° to 25°. As described previously, a positive difference means that the AMSU wind at 850 hPa turns less inward toward the TC center than does the QuikSCAT surface wind. To adjust the AMSU wind direction at 850 hPa to the surface wind, the direction must be turned inward slightly.

The same trend is found for the dependence of the AMSU–H*Wind direction difference on the AMSU wind speed, except for a small negative bias at the lowest AMSU wind speeds in Fig. 5 and Table 3.

From these comparisons described above, the AMSU winds have some systematic differences from the QuikSCAT and H*Wind winds. The wind speed differences between the AMSU wind at 850 hPa and the surface winds are proportional to the AMSU wind speed itself. The wind direction differences of AMSU and the two surface wind datasets also have biases that depend on the AMSU wind speed. Using these relationships, the TC surface wind distribution retrieved from the 850-hPa AMSU winds can be converted to surface wind. The surface wind speed is retrieved from the AMSU wind speed at 850 hPa with a regression model. The surface wind direction is obtained from the AMSU wind direction at 850 hPa minus the bias as a function of the AMSU wind speed. Two sets of AMSU surface wind adjustment relationships were derived. The adjustments derived from the AMSU–QuikSCAT comparison are called QCOM (Table 4) and the adjustments from H*Wind are called HCOM (Table 5). In the relationships shown in Tables 4 and 5, WSsurf means surface wind speed, and WSamsu means AMSU wind speed at 850 hPa; WD (°) is the abbreviation for wind direction, and subscripts are the same as for WS (m s^{-1}). Validations of these relationships applied to the AMSU 850-hPa winds to provide surface winds are described in the next section for two independent cases.

5. Validations of retrieval methods of surface wind

To validate the QCOM and HCOM adjustments, these methods are applied to AMSU wind fields at 850 hPa and compared with corresponding QuikSCAT and

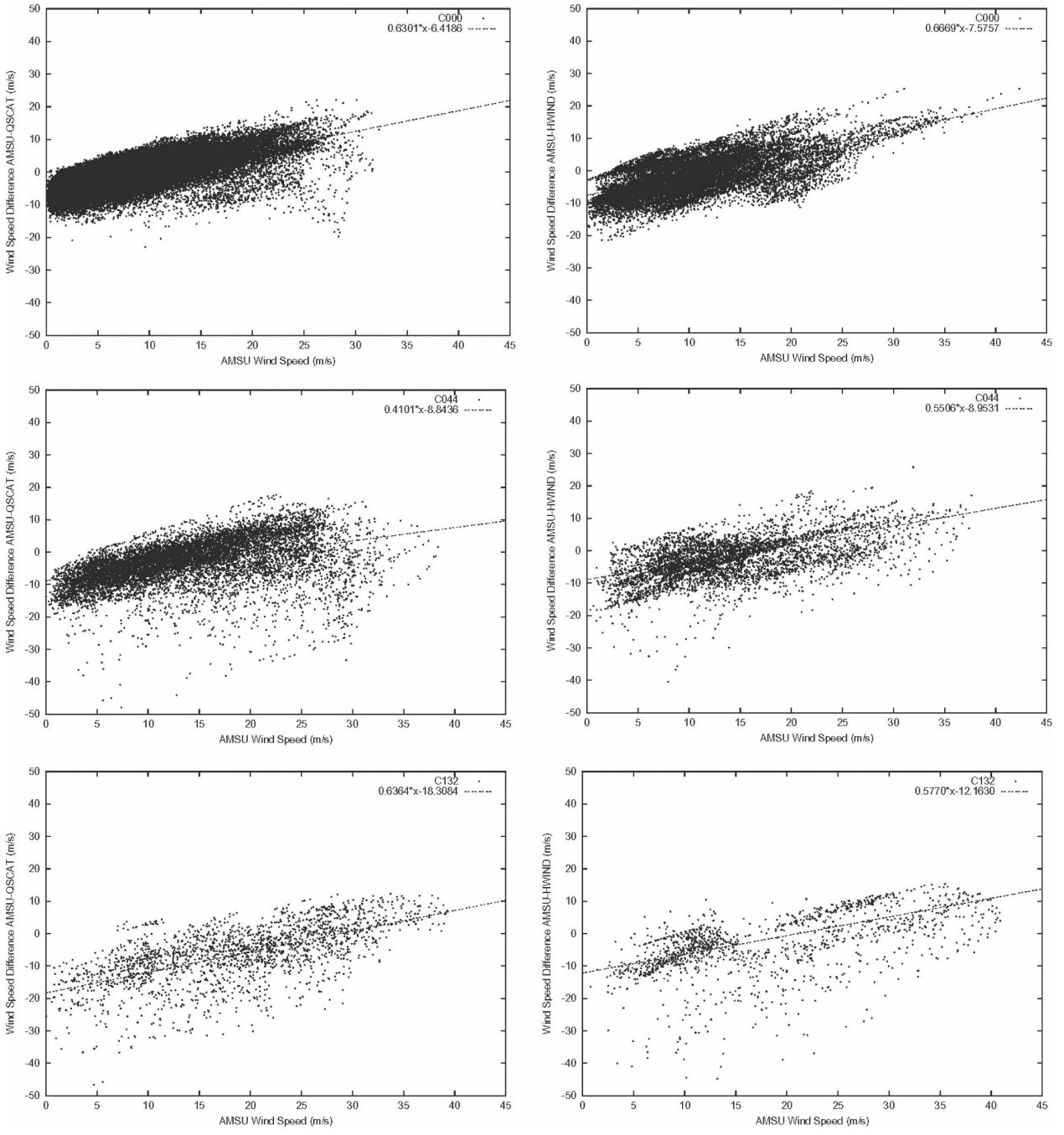

FIG. 4. (left) Scatter diagrams of 850-hPa AMSU wind speed vs 850-hPa AMSU wind speed minus QuikSCAT surface wind speed, and (right) diagrams of 850-hPa AMSU wind speed vs 850-hPa AMSU wind speed minus H*Wind surface wind speed; points with (top) CLW $<$ 0.44 mm, (middle) 0.44 mm $\leq$ CLW $<$ 1.32 mm, and (bottom) CLW $\geq$ 1.32 mm.

H*Wind surface wind fields. For these comparisons, the two cases in which all three types of wind data were obtained simultaneously are used. The first case is from Hurricane Floyd (1999) observed by AMSU at 2332 UTC 11 September, by QuikSCAT at 2221 UTC 11 September, and by H*Wind at 0130 UTC 12 September. The second case is from Hurricane Michelle (2001) observed by AMSU at 0023 UTC 3 November, by QuikSCAT at 2319 UTC 2 November, and by H*Wind at 0130 UTC 3 November. As described in section 3 these were the only two cases in the 1999–2002 sample that were away from major landmasses and had all

TABLE 3. Statistics of the comparisons of AMSU wind speed at 850 hPa with the wind speed difference between AMSU at 850 hPa and QuikSCAT or H*Wind surface winds, stratified by cloud liquid water amount.

	No. of data	Slope	Intercept	COR
QuikSCAT				
CLW $<$ 0.44 mm	72 166	0.63	−6.42	0.709
0.44 mm $\leq$ CLW $<$ 1.32 mm	10 466	0.41	−8.84	0.439
1.32 mm $\leq$ CLW	1964	0.64	−18.31	0.624
H*Wind				
CLW $<$ 0.44 mm	16 265	0.67	−7.58	0.695
0.44 mm $\leq$ CLW $<$ 1.32 mm	4618	0.55	−8.95	0.627
1.32 mm $\leq$ CLW	1334	0.58	−12.16	0.612

three data types available. These two cases were withheld from the development of the QCOM and HCOM relationships to provide an independent sample. As a third wind estimate, NCEP global model surface analyses are also used to assess the quality of the QCOM and HCOM adjustments. NCEP analyses for the validation are at 0000 UTC 12 September for Floyd and 0000 UTC 3 November for Michelle. The purpose of including the NCEP winds is to determine if the AMSU algorithm has any advantage over what is possible from the assimilation of operational data sources. The AMSU surface wind fields could also have been compared with in situ wind data such as buoys. However, these data are very sparse, and the H*Wind analyses already include them when available.

Figure 6 shows the wind fields for Floyd from AMSU at 850 hPa (Fig. 6a), QuikSCAT (Fig. 6b), H*Wind (Fig. 6c), and NCEP (Fig. 6d). The CLW field estimated from AMSU is also shown in Fig. 7. The 850-hPa AMSU wind field in Fig. 6a does not include the modification by QCOM or HCOM (hereinafter NOMO). The wind speed distribution of AMSU above 12 m s^{-1} is similar to the wind speed distribution of QuikSCAT (Fig. 6b). The high-speed region is asymmetric and is located in the direction from north to southeast of the hurricane center, similar to a rainband. The distribution

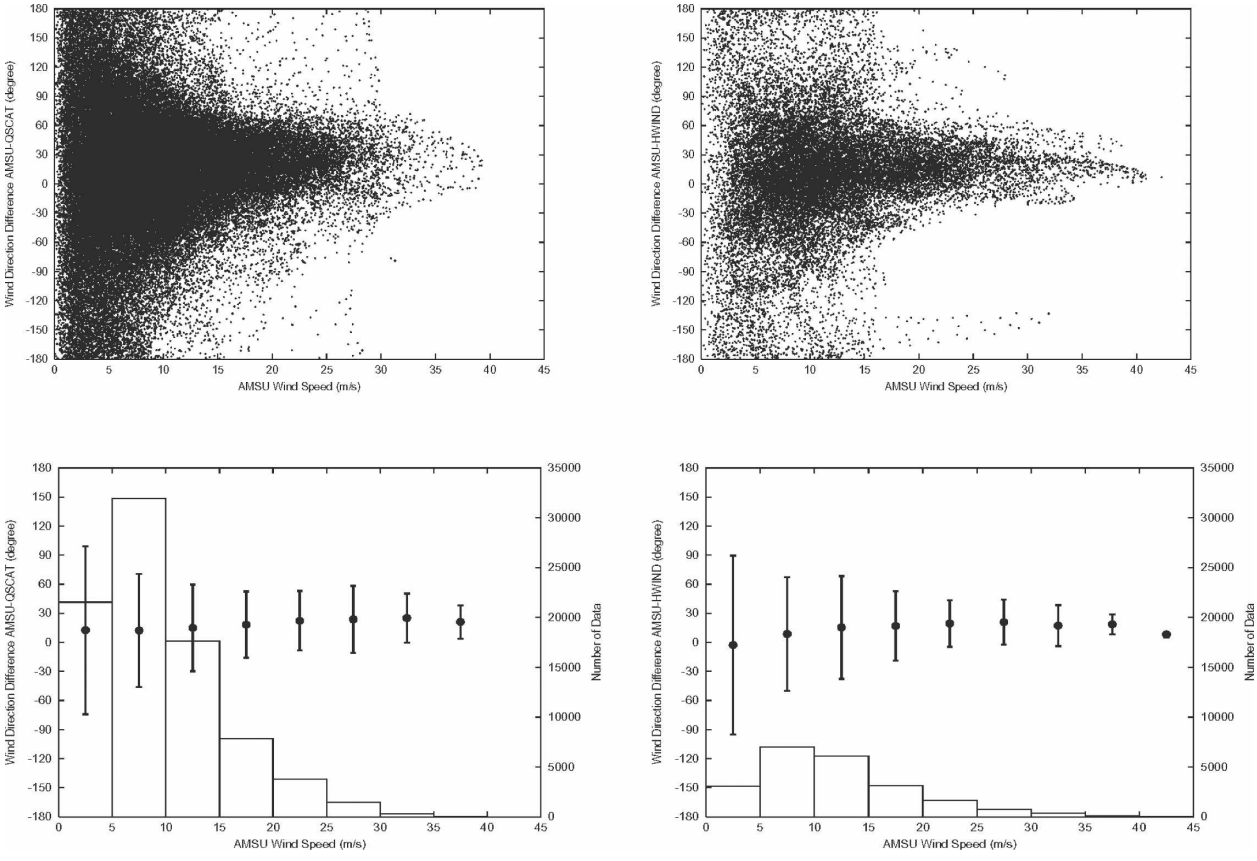

FIG. 5. Scatter diagrams of 850-hPa AMSU wind speed vs 850-hPa AMSU wind directions (top left) minus QuikSCAT surface wind direction and (top right) minus H*Wind surface wind direction. (bottom) Histograms of the total grid numbers, the mean wind direction differences, and bars of standard deviation of the wind direction differences in 5 m s^{-1} intervals of 850-hPa AMSU wind speeds: comparison with (bottom left) QuikSCAT and (bottom right) H*Wind.

TABLE 4. QCOM: surface wind retrieval method derived from comparison with QuikSCAT.

WS	
WSsurf = [(1 − 0.63) × WSamsu] + 6.42	(CLW < 0.44 mm)
WSsurf = [(1 − 0.41) × WSamsu] + 8.84	(0.44 ≤ CLW < 1.32 mm)
WSsurf = [(1 − 0.64) × WSamsu] + 18.31	(1.32 ≤ CLW mm)
WD	
WDsurf = WDamsu − 12.60	(WSamsu < 5 m s^{-1})
WDsurf = WDamsu − 12.30	(5 ≤ WSamsu < 10 m s^{-1})
WDsurf = WDamsu − 15.02	(10 ≤ WSamsu < 15 m s^{-1})
WDsurf = WDamsu − 18.30	(15 ≤ WSamsu < 20 m s^{-1})
WDsurf = WDamsu − 22.35	(20 ≤ WSamsu < 25 m s^{-1})
WDsurf = WDamsu − 23.81	(25 ≤ WSamsu < 30 m s^{-1})
WDsurf = WDamsu − 25.08	(30 ≤ WSamsu < 35 m s^{-1})
WDsurf = WDamsu − 21.08	(35 ≤ WSamsu)

of CLW roughly corresponds to the distributions of wind speed above 12 m s^{-1} (Fig. 7). The AMSU wind speed distribution above 18 m s^{-1} is wider along the direction from north to south than that of QuikSCAT winds. It can also be seen that the AMSU wind speed distribution above 18 m s^{-1} is narrower in the east–west direction than that of QuikSCAT. The AMSU wind speed field has some patches of weak speed below 2 m s^{-1} located on the west side of the strong wind speed area already mentioned. The H*Wind wind speed distribution in Fig. 6c is different from those of AMSU or QuikSCAT. The wind speed distribution of H*Wind is almost symmetric, and there is no band-type high wind speed area in the distribution. Thus, neither the AMSU nor QuikSCAT retrievals are able to capture the intense inner core of the storm because of the horizontal resolution limitations described previously. The NCEP surface wind analysis also shows an asymmetric distribution, which is similar to those of AMSU and QuikSCAT (Fig. 6d).

TABLE 5. HCOM: same as Table 4, but for H*Wind.

WS	
WSsurf = [(1 − 0.67) × WSamsu] + 7.58	(CLW < 0.44 mm)
WSsurf = [(1 − 0.55) × WSamsu] + 8.95	(0.44 ≤ CLW < 1.32 mm)
WSsurf = [(1 − 0.58) × WSamsu] + 12.16	(1.32 ≤ CLW mm)
WD	
WDsurf = WDamsu + 2.78	(WSamsu < 5 m s^{-1})
WDsurf = WDamsu − 8.62	(5 ≤ WSamsu < 10 m s^{-1})
WDsurf = WDamsu − 15.34	(10 ≤ WSamsu < 15 m s^{-1})
WDsurf = WDamsu − 16.98	(15 ≤ WSamsu < 20 m s^{-1})
WDsurf = WDamsu − 19.45	(20 ≤ WSamsu < 25 m s^{-1})
WDsurf = WDamsu − 20.92	(25 ≤ WSamsu < 30 m s^{-1})
WDsurf = WDamsu − 17.29	(30 ≤ WSamsu < 35 m s^{-1})
WDsurf = WDamsu − 18.67	(35 ≤ WSamsu < 40 m s^{-1})
WDsurf = WDamsu − 8.28	(40 ≤ WSamsu m s^{-1})

The AMSU wind direction near the hurricane center has a structure similar to that for QuikSCAT, H*Wind, and NCEP, with a general counterclockwise rotation. However, in the outer region of the hurricane center the AMSU wind direction distribution shows remarkable differences from those of QuikSCAT, H*Wind, and NCEP, which still show counterclockwise circulations away from the storm center. Especially in the weak wind speed regions of AMSU there are some small vortices, which are widely different from an ideal distribution of wind direction in TCs. The small vortices are likely artifacts of the AMSU retrieval technique because of the problems of liquid water attenuation or ice scattering.

The wind fields from the four data types for the Hurricane Michelle case (not shown) are fairly similar to the results for Floyd. Generally, the two satellite wind fields show similar structures, where the high wind speed region is located on the periphery of the hurricane center with speeds lower than in the H*Wind analyses, and the speed gradually decreases away from the storm center. Wind directions show counterclockwise circulation near the storm center. The NCEP surface wind field for the Michelle case is different from other three wind fields. The center of rotation of Michelle in the NCEP wind field is located on northeastern side of those of other three wind fields. The AMSU wind speed distribution shows several weak speed patches below 6 m s^{-1} away from the hurricane center, with small vortices similar to those in the Floyd case. These features were not seen in the QuikSCAT, H*Wind, or NCEP wind fields.

Figure 8 shows the surface wind field retrieved from the AMSU wind at 850 hPa using the QCOM (Fig. 8a) and HCOM (Fig. 8b) adjustments for the Floyd case. When QCOM is compared with the QuikSCAT surface image (Fig. 6b), it is easily seen that the wind speed distribution of QCOM more closely resembles that of QuikSCAT than the original AMSU wind field (NOMO). It has also similar characters with the NCEP wind field. In QCOM, the wind speed area above 12 m s^{-1} spreads in the east–west direction, but the strongest wind region above 24 m s^{-1} is shortened in the north–south direction. The weak wind speed patches away from the hurricane center in NOMO have almost disappeared in QCOM. Similar tendencies are also found in HCOM, but the strongest wind region near the center has shrunk excessively. The asymmetric wind speed distribution of QCOM and HCOM are still considerably different from the very symmetric H*Wind distribution.

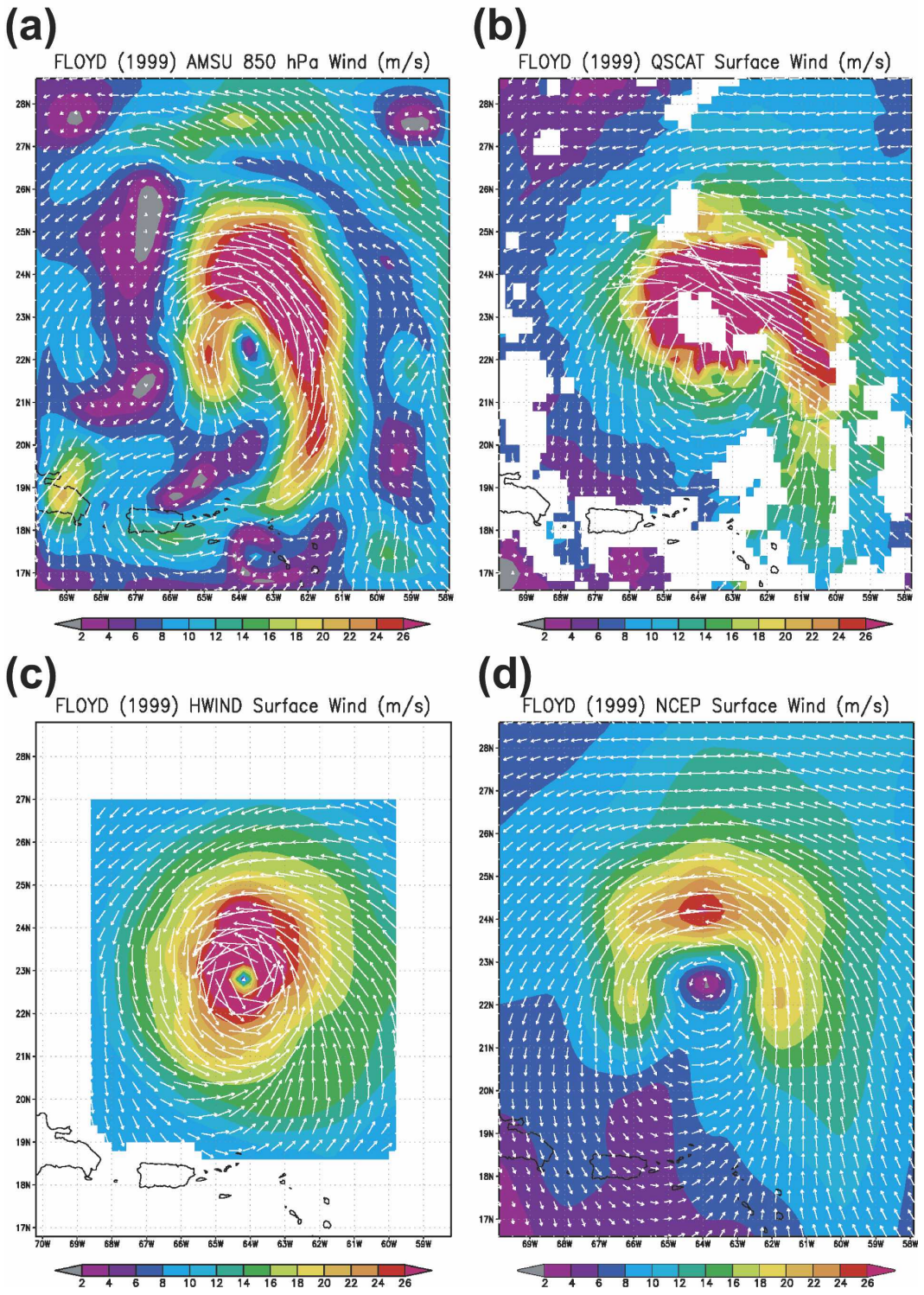

FIG. 6. (a) The 850-hPa AMSU wind distribution, (b) QuikSCAT surface wind distribution, (c) H*Wind surface wind distribution, and (d) surface wind distribution of NCEP global model analyses for Hurricane Floyd (1999). The contour interval for wind speed is 2 m s^{-1}. The wind direction is indicated by the white arrows, and the arrow length is proportional to the wind speed.

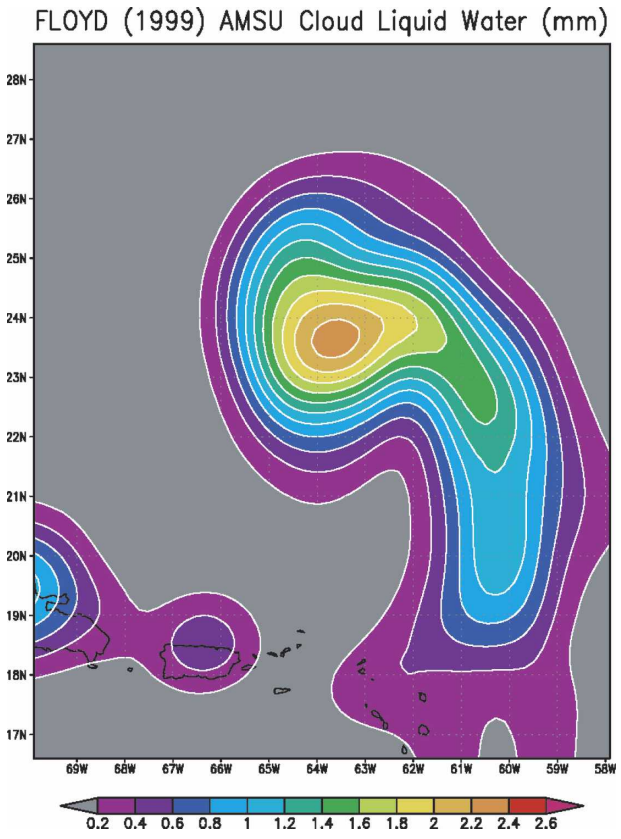

FIG. 7. AMSU cloud liquid water distribution for Hurricane Floyd (1999). The contour interval for CLW is 2 mm.

Wind direction differences away from the hurricane center of QCOM or HCOM become smaller than that of NOMO as compared with the QuikSCAT, H*Wind, or NCEP surface winds. However, the small vortices, corresponding to weak wind speed regions located on the west side of the periphery of the center, still exist in QCOM and HCOM.

The QCOM and HCOM surface winds for the Michelle case were also compared with the QuikSCAT, H*Wind, NCEP, or NOMO wind fields (not shown), and the results were similar to the Floyd case. The strong wind speed distribution in QCOM is more similar to that of QuikSCAT and H*Wind than NOMO. The NCEP surface wind field for the Michelle case did not resemble the QCOM field. The weak wind regions on periphery of the center were reduced in QCOM, but the small vortices seen in NOMO still exist. HCOM shows the same features as QCOM except for the maximum wind speed, which is lower than that of QCOM.

Table 6 shows statistical results for comparisons of the three kinds of AMSU wind retrievals (NOMO, QCOM, and HCOM) and the surface winds of QuikSCAT for the combined sample from Hurricanes Floyd and Michelle. Statistics of the comparisons of the surface wind of NCEP with the surface wind of QuikSCAT for the cases of Hurricanes Floyd and Michelle are also shown as reference. This table shows that the QCOM adjustment improves the AMSU wind speed retrieval relative to the NOMO case. The NOMO correlation coefficient and MAD are 0.589 and 5.48 m s^{-1}, respectively. For QCOM, the correlation coefficient increases to 0.776 and the MAD is reduced to 3.40 m s^{-1}. The wind speed improvements for the HCOM adjustments are similar to (but not quite as good as) those for QCOM, with a correlation coefficient and MAD of 0.753 and 3.58 m s^{-1}, respectively. The NCEP wind speed MAD from QuikSCAT is comparable to that from NOMO and a little larger than those for QCOM and HCOM.

The improvements in the AMSU wind direction for the QCOM or HCOM adjustments are not as good as those for wind speed. The MAD for NOMO in Table 6 is 34.4°, which reduces only slightly to 33.6° and 33.0° for QCOM and HCOM, respectively. The correlation coefficients for QCOM and HCOM are a little smaller than that for NOMO. The NCEP wind directions shows better results than do those of QCOM and HCOM, especially for the MAD and the correlation coefficients. The differences between the results of three kinds of AMSU winds (NOMO, QCOM, and HCOM) and NCEP surface winds are probably because of the spurious vortices away from the storm center in the AMSU analyses. These results indicate that the simple algorithm to modify the AMSU wind direction by subtracting the bias as a function of AMSU wind speed has some limitations.

The results from comparisons between the H*Wind surface wind and three AMSU wind fields (NOMO, QCOM, and HCOM) are shown in Table 7. The statistical results from comparisons between the H*Wind and NCEP surface winds are also shown. The results generally are similar to those for the comparison with QuikSCAT in that the QCOM and HCOM procedures improve the wind speed error more than the wind direction error. However, the correlation coefficients are smaller and the MADs are larger in the comparisons with H*Wind than in those with QuikSCAT. This degradation in the comparison is primarily because of the fact that the H*Wind analyses resolve the inner core of the storm, but the AMSU and QuikSCAT analyses do not. Similar to the comparison with QuikSCAT, NCEP shows comparable results to QCOM and HCOM in the MAD for wind speed, and better results than QCOM and HCOM in the MAD and the correlation coefficients for wind direction. Because of the aircraft data in H*Wind, the comparisons with AMSU and NCEP are

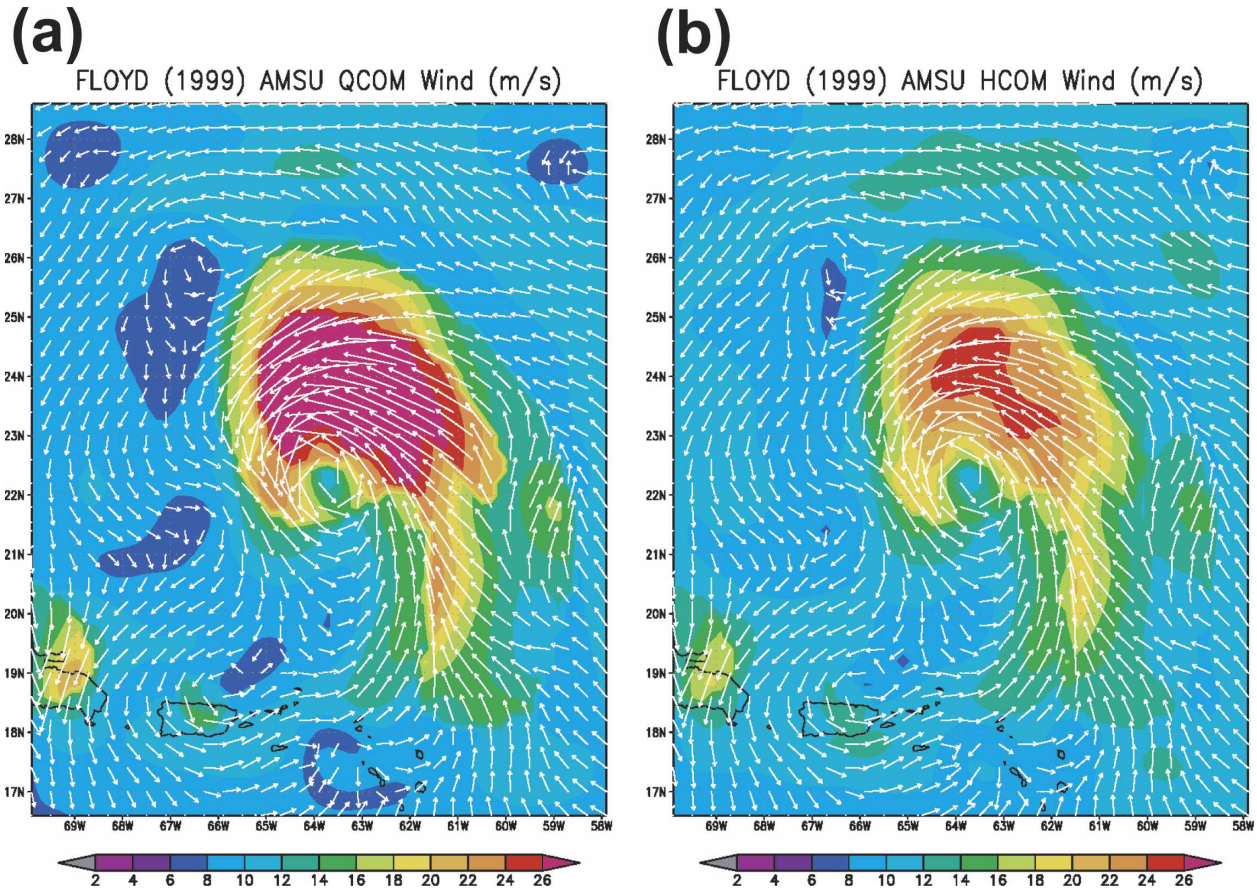

FIG. 8. Surface wind distributions estimated by (a) QCOM and (b) HCOM. Contours and arrows are the same as in Fig. 6.

measures of the accuracies of these two methods. This result indicates that in the vicinity of TCs, the AMSU retrievals have comparable accuracy to global data assimilation systems.

Table 8 shows the results from comparisons between the NCEP surface wind and the three AMSU wind fields (NOMO, QCOM, and HCOM). Almost the same results are found in this table as previously mentioned in the discussion of Tables 6 and 7. QCOM and HCOM improve the correlation coefficients for wind speed, but the values of the coefficients are lower than other two validations with QuikSCAT and H*Wind. The wind direction retrieval algorithm in QCOM and HCOM again do not show much improvement. In these statistics, the bias of wind direction in QCOM and HCOM shows the same (but negative) magnitude as that in NOMO.

6. Discussion

One purpose of this paper is a comparison of the wind field retrieved from AMSU temperature data using the nonlinear balance equation at 850 hPa with surface wind fields obtained from QuikSCAT or H*Wind. The second objective is to use the results of the com-

TABLE 6. Statistics of the comparisons of the three kinds of AMSU wind with the surface wind of QuikSCAT for the cases of Hurricanes Floyd (1999) and Michelle (2001). Statistics of the comparisons of NCEP surface wind with QuikSCAT are also shown for reference.

	No. of data	Bias	MAD	COR
850-hPa wind (NOMO)				
Wind speed (m s^{-1})	2514	−1.94	5.48	0.589
Wind direction (°)	2514	11.8	34.4	0.803
QCOM				
Wind speed (m s^{-1})	2514	−0.49	3.40	0.776
Wind direction (°)	2514	−4.4	33.6	0.794
HCOM				
Wind speed (m s^{-1})	2514	−1.11	3.58	0.753
Wind direction (°)	2514	−0.9	33.0	0.792
NCEP				
Wind speed (m s^{-1})	2514	−1.94	3.83	0.593
Wind direction (°)	2514	2.3	17.8	0.919

TABLE 7. Same as Table 6, but for H*Wind.

	No. of data	Bias	MAD	COR
850-hPa wind (NOMO)				
Wind speed (m s^{-1})	2916	−0.10	5.97	0.461
Wind direction (°)	2916	15.7	29.5	0.784
QCOM				
Wind speed (m s^{-1})	2916	1.36	4.63	0.612
Wind direction (°)	2916	−0.7	28.5	0.781
HCOM				
Wind speed (m s^{-1})	2916	0.70	4.25	0.594
Wind direction (°)	2916	2.7	28.0	0.783
NCEP				
Wind speed (m s^{-1})	2916	−0.42	4.36	0.454
Wind direction (°)	2916	11.8	19.0	0.921

parison to develop an adjustment procedure for reducing the AMSU 850-hPa winds to the surface, and then to evaluate the adjustment procedure on independent cases.

The estimation of surface wind speed using the adjustment procedure showed positive results. The correlation coefficients increased and the wind speed errors decreased after the adjustments were applied, when AMSU wind fields were compared with those from QuikSCAT, H*Wind, or NCEP. Franklin et al. (2003) show the mean vertical profile of wind speed in hurricanes obtained from GPS dropwindsonde from the surface to 700 hPa. Their results confirmed recent operational procedures to estimate surface winds from flight-level winds. In their study, they proposed that reduction factors be multiplied by aircraft wind speeds at 850 or 700 hPa to estimate the surface wind speed. The surface adjustments using the regression equations in this paper have some similarities with those described by Franklin et al. (2003). However, according to Kepert (2001) and Kepert and Wang (2001), the use of universal constants for adjustment factors to reduce the surface wind speed is incorrect. In this paper, the adjustment factors are a function of CLW. The reduction factors used by Franklin et al. (2003) are below 1.0, which means that the surface wind speeds are always less than those at 850 or 700 hPa. This type of procedure would not work well for adjusting the AMSU data to the surface because the adjustment procedure also corrects for a speed bias that is function of the AMSU wind speed. As seen in the wind speed formulas in Tables 4 and 5, the AMSU adjustment procedure acts to increase (decrease) the AMSU wind speeds at 850 hPa when the AMSU speeds are lower (higher) than a certain wind speed value to estimate of surface wind speed.

TABLE 8. Same as Table 6, but for NCEP.

	No. of data	Bias	MAD	COR
850-hPa wind (NOMO)				
Wind speed (m s^{-1})	3404	0.10	5.24	0.453
Wind direction (°)	3404	7.8	35.6	0.630
QCOM				
Wind speed (m s^{-1})	3404	1.66	3.89	0.545
Wind direction (°)	3404	−8.5	37.4	0.626
HCOM				
Wind speed (m s^{-1})	3404	1.21	3.19	0.542
Wind direction (°)	3404	−5.2	36.6	0.628

Powell and Black (1990) showed that low-level atmospheric stability has a strong influence on surface wind speeds in TCs. They found different reduction factors from the flight-level wind speed to the surface in stable, unstable, and neutral conditions. However, the QuikSCAT surface wind speeds are retrieved assuming neutral stratification. In this paper, atmospheric stratification is not considered in the development of the AMSU adjustment procedure from wind speeds at 850 hPa to the surface. As a next step, this issue should be considered to refine the AMSU wind speed adjustment procedure using the sea surface temperature and the low-level atmospheric temperature.

There are some problems in the wind direction estimated by AMSU. As seen in Fig. 6a, the AMSU wind field at 850 hPa has several small vortices away from the storm center, which is not realistic in a TC, and were not seen in the corresponding QuikSCAT, H*Wind, or NCEP analyses. It can be seen in the comparison of Fig. 6a and 7 that these small vortices are located on the periphery of areas of higher CLW, or near land. Thus, they are likely results from errors in the AMSU temperature retrieval algorithm in these areas. Further work is needed to remove these "contamination" effects from AMSU brightness temperature data, so that the nonlinear balance equation will produce more realistic flow around a TC without these small vortices being created.

Another problem is the bias-removing algorithm for adjusting the AMSU wind directions to the surface. In the validation for Hurricanes Floyd and Michelle it was found that wind directions in the strong wind speed regions were improved by the QCOM and HCOM procedures. However, in the weak speed areas, such as in the vicinity of the small vortices, the wind directions in QCOM and HCOM do not correspond to the surface wind directions of the QuikSCAT, H*Wind, or NCEP analyses. The correlation coefficient and MAD of wind direction for QCOM and HCOM with QuikSCAT, H*Wind, or NCEP do not show any significant improvements relative to the unadjusted AMSU wind directions. This lack of improvement indicates that the

bias-removing method is of limited usefulness for reducing the AMSU directions to the surface. The adjustment does, however, provide a better estimate of the inflow angle of the surface wind relative to the 850-hPa wind in an area-averaged sense.

Further improvements in the estimation of surface wind direction from the 850-hPa AMSU wind direction will require an analysis of the relation between the wind direction difference and additional physical parameters such as vertical wind shear, direction of TC motion, convective activity around the TCs, and so on. It will also be necessary to derive a regression model between wind direction and wind speed, or CLW using circular statistics.

Although the AMSU surface wind algorithm still has some problems, especially for the wind direction, the results show that the wind speeds compare well with QuikSCAT. The QuikSCAT winds also sometimes have large errors in the wind direction estimates, especially near the center and the edges of the wind swath. Even with these errors, QuikSCAT has proved to be very useful for TC analysis, especially away from the inner core. Thus, the AMSU surface winds should have similar utility.

In future studies, the problems above mentioned will be further investigated. The effectiveness and impact of the AMSU surface wind will be investigated, particularly in the periphery and center region of TCs. In addition, the accuracy of the AMSU surface winds in different parts of the storm will be studied (e.g., in the inner core versus the outer part of the storm). It may be possible to combine the AMSU winds in the areas where they are most accurate with parameters derived from other instruments or numerical model fields.

Zhu et al. (2002) showed that a hurricane bogus vortex derived from three-dimensional AMSU observations can have a large impact on the numerical TC prediction. Their algorithm for making a vortex from AMSU data is similar to the method described here for the 850-hPa AMSU winds. However, Zhu et al. (2002) do not include a surface wind field estimate. Applying our method to generate a bogus vortex for numerical TC prediction model initialization may help to further improve the forecast results of Zhu et al. (2002).

AMSUs are now on board the current series of NOAA operational polar-orbiting satellites and the data are available in real time on operational centers. If the surface wind retrieval algorithm in this paper works suitably, diagnosing the wind field of TCs from AMSU will be practical in routine TC analysis and prediction models in the near future. Similar to QuikSCAT, it should be especially useful for TCs in most ocean basins that do not have routine aircraft reconnaissance.

7. Summary

AMSU-retrieved wind fields at 850 hPa were compared with the surface wind fields from QuikSCAT and H*Wind. From these comparisons, it was found that the AMSU wind speed at 850 hPa has a linear relationship with the surface wind speed of QuikSCAT or H*Wind. The characteristic bias of wind direction also appeared between AMSU and QuikSCAT or H*Wind. Applying regression models for adjusting AMSU wind speeds and the bias-removing method for AMSU wind directions, an algorithm was developed to estimate the surface wind field from the AMSU wind at 850 hPa. This algorithm was simple but robust, especially for wind speed.

The algorithm was validated in two independent cases from Hurricanes Floyd and Michelle, which were simultaneously observed by AMSU, QuikSCAT, and H*Wind. In this validation the regression model for wind speeds showed positive results. On the other hand, the bias-removing method for wind direction has room for improvement.

Acknowledgments. The authors thank Julie Demuth for her helpful discussions. Kotaro Bessho's contribution was performed during a visit to CIRA/CSU as an affiliated scientist supported by the Ministry of Education, Culture, Sports, Science and Technology of the Japanese Government. The views, opinions, and findings in this report are those of the authors and should not be construed as an official NOAA and/or U.S. government position, policy, or decision.

REFERENCES

Barnes, S. L., 1964: A technique for maximizing details in numerical weather map analysis. *J. Appl. Meteor.,* **3,** 396–409.

Brueske, K. F., and C. S. Velden, 2003: Satellite-based tropical cyclone intensity estimation using the NOAA-KLM series Advanced Microwave Sounding Unit (AMSU). *Mon. Wea. Rev.,* **131,** 687–697.

Charney, J., 1955: The use of the primitive equations of motion in numerical prediction. *Tellus,* **7,** 22–26.

Demuth, J. L., M. DeMaria, J. A. Knaff, and T. H. Vonder Haar, 2004: Evaluation of Advanced Microwave Sounding Unit tropical-cyclone intensity and size estimation algorithms. *J. Appl. Meteor.,* **43,** 282–296.

Dvorak, V. F., 1975: Tropical cyclone intensity analysis and forecasting from satellite imagery. *Mon. Wea. Rev.,* **103,** 420–430.

——, 1984: Tropical cyclone intensity analysis using satellite data. NOAA Tech. Rep. NESDIS 11, 47 pp.

Fisher, N. I., 1993: *Statistical Analysis of Circular Data.* Cambridge University Press, 296 pp.

Frank, W. M., 1977: The structure and energetics of the tropical cyclone. I. Storm structure. *Mon. Wea. Rev.,* **105,** 1119–1135.

Franklin, J. L., M. L. Black, and K. Valde, 2003: GPS dropwind-

sonde wind profiles in hurricanes and their operational implications. *Wea. Forecasting,* **18,** 32–44.

Iversen, T., and T. E. Nordeng, 1982: A convergent method for solving the balance equation. *Mon. Wea. Rev.,* **110,** 1347–1353.

Jammalamadaka, S. R., and A. SenGupta, 2001: *Topics in Circular Statistics.* World Scientific, 336 pp.

Kasahara, A., 1982: Significance of non-elliptic regions in balance flows of the tropical atmosphere. *Mon. Wea. Rev.,* **110,** 1956–1967.

Katsaros, K. B., E. B. Forde, P. Chang, and W. T. Liu, 2001: QuikSCAT's SeaWinds facilitates early identification of tropical depressions in 1999 hurricane season. *Geophys. Res. Lett.,* **28,** 1043–1046.

Kepert, J., 2001: The dynamics of boundary layer jets within the tropical cyclone core. Part I: Linear theory. *J. Atmos. Sci.,* **58,** 2469–2484.

——, and Y. Wang, 2001: The dynamics of boundary layer jets within the tropical cyclone core. Part II: Nonlinear enhancement. *J. Atmos. Sci.,* **58,** 2485–2501.

Kidder, S. Q., W. M. Gray, and T. H. Vonder Haar, 1978: Estimating tropical cyclone central pressure and outer winds from satellite microwave data. *Mon. Wea. Rev.,* **106,** 1458–1464.

——, ——, and ——, 1980: Tropical cyclone outer surface winds derived from satellite microwave sounder data. *Mon. Wea. Rev.,* **108,** 144–152.

——, M. D. Goldberg, R. M. Zehr, M. DeMaria, J. F. W. Purdom, C. S. Velden, N. C. Grody, and S. J. Kusselson, 2000: Satellite analysis of tropical cyclones using the Advanced Microwave Sounding Unit (AMSU). *Bull. Amer. Meteor. Soc.,* **81,** 1241–1259.

Knaff, J. A., R. M. Zehr, M. D. Goldberg, and S. Q. Kidder, 2000: An example of temperature structure differences in two cyclone systems derived from the Advanced Microwave Sounding Unit. *Wea. Forecasting,* **15,** 476–483.

Linstid, B., 2000: An algorithm for the correction of corrupted AMSU temperature data in tropical cyclones. M.S. thesis, Department of Mathematics, Colorado State University, 24 pp.

Merrill, R. T., 1995: Simulations of physical retrieval of tropical cyclone thermal structure using 55-GHz band passive microwave observations from polar-orbiting satellites. *J. Appl. Meteor.,* **34,** 773–787.

Negri, A. J., and R. F. Adler, 1993: An intercomparison of three satellite infrared rainfall techniques over Japan and surrounding waters. *J. Appl. Meteor.,* **32,** 357–373.

Paegle, J., and J. N. Paegle, 1976: On geopotential data and ellipticity of the balance equation: A data study. *Mon. Wea. Rev.,* **104,** 1279–1288.

Powell, M. D., 1980: Evaluations of diagnostic marine boundary-layer models applied to hurricanes. *Mon. Wea. Rev.,* **108,** 757–766.

——, and P. G. Black, 1990: The relationship of hurricane reconnaissance flight-level wind measurements to wind measured by NOAA's oceanic platforms. *J. Wind Eng. Ind. Aerodyn.,* **36,** 381–392.

——, and S. H. Houston, 1996: Hurricane Andrew's landfall in south Florida. Part II: Surface wind fields and potential real-time applications. *Wea. Forecasting,* **11,** 329–349.

——, ——, and T. A. Reinhold, 1996: Hurricane Andrew's landfall in South Florida. Part I: Standardizing measurements for documentation of surface wind fields. *Wea. Forecasting,* **11,** 304–328.

——, ——, L. R. Amat, and N. Morisseau-Leroy, 1998: The HRD real-time hurricane wind analysis system. *J. Wind Eng. Ind. Aerodyn.,* **77–78,** 53–64.

Quilfen, Y., B. Chapron, T. Elfouhaily, K. Katsaros, and J. Tournadre, 1998: Observation of tropical cyclones by high-resolution scatterometry. *J. Geophys. Res.,* **103** (C4), 7767–7786.

Spencer, R. W., and W. D. Braswell, 2001: Atlantic tropical cyclone monitoring with AMSU-A: Estimation of maximum sustained wind speeds. *Mon. Wea. Rev.,* **129,** 1518–1532.

Velden, C. S., 1989: Observational analyses of North Atlantic tropical cyclones from NOAA polar-orbiting satellite microwave data. *J. Appl. Meteor.,* **28,** 59–70.

——, and W. L. Smith, 1983: Monitoring tropical cyclone evolution with NOAA satellite microwave observations. *J. Climate Appl. Meteor.,* **22,** 714–724.

——, B. M. Goodman, and R. T. Merrill, 1991: Western North Pacific tropical cyclone intensity estimation from NOAA polar-orbiting satellite microwave data. *Mon. Wea. Rev.,* **119,** 159–168.

Wentz, F. J., D. K. Smith, C. A. Mears, and C. L. Gentemann, 2001: Advanced algorithms for QuikScat and SeaWinds/AMSR. *Proc. Int. Geoscience and Remote Sensing Symp. 2001 (IGARSS '01),* Vol. 3, Sydney, Australia, IEEE, 1079–1081.

Zhu, T., D. L. Zhang, and F. Weng, 2002: Impact of the Advanced Microwave Sounding Unit measurements on hurricane prediction. *Mon. Wea. Rev.,* **130,** 2416–2432.